

# Colloquium: Laws controlling crystallization and melting in bulk polymers

Gert Strobl\*

*Physikalisches Institut, Albert-Ludwigs-Universität Freiburg, 79104 Freiburg, Germany*

(Published 10 September 2009)

After the fundamental structure of semicrystalline polymers—platelike crystallites with thicknesses in the nanometer range, embedded in a liquid matrix—was discovered in the late 1950s, attention turned to the mechanism of formation. After intense controversial discussions, an approach put forward by Hoffman and Lauritzen prevailed and was broadly accepted. The picture envisaged by the treatment—platelike crystallites with atomically smooth side faces and a surface occupied by chain folds, growing sideways layer by layer with a secondary nucleation as the rate-determining step—was easy to grasp and yielded simple relationships. The main control parameter is the supercooling below the equilibrium melting point of a macroscopic crystal  $T_f^\infty$ , which determines both the thickness of the crystallites and their lateral growth rate. The impression that the mechanism of polymer crystallization was understood and the issue essentially settled, however, was wrong. Experiments carried out during the last decade on various polymer systems provided new insights which are now completely changing our understanding of such systems. They revealed a number of laws that control polymer crystallization and melting in bulk, showing in particular that the crystal thickness is inversely proportional to the distance to a temperature  $T_c^\infty$  which is located above the equilibrium melting point, and that crystal growth stops at a temperature  $T_{zg}$  which is below  $T_f^\infty$ . Observations indicate that the pathway followed in the growth of polymer crystallites includes an intermediate metastable phase. In a proposed model a thin layer with mesomorphic inner structure forms between the lateral crystal face and the melt. The first step in the growth process is attachment of the coiled chain sequences of the melt onto the mesomorphic layer, which subsequently is transformed into the crystalline state. The transitions between melt, mesomorphic layers, and lamellar crystallites can be described with the aid of a temperature-thickness phase diagram.  $T_c^\infty$  and  $T_{zg}$  are identified with the temperatures of the (hidden) transitions between the mesomorphic and the crystalline phase, and between the liquid and the mesomorphic phase, respectively. Comparing predictions of the model theory with experimental results from small-angle x-ray scattering, optical microscopy, and calorimetry yields in addition to the three equilibrium transition temperatures latent heats of transition and surface free energies.

DOI: [10.1103/RevModPhys.81.1287](https://doi.org/10.1103/RevModPhys.81.1287)

PACS number(s): 61.41.+e, 64.70.km, 81.10.Aj, 81.30.Fb

## CONTENTS

I. Introduction	1287
II. Conventional Views: The Hoffman-Lauritzen Model	1289
III. New Experimental Results	1290
A. Crystallization line, recrystallization line, and melting line	1290
B. Granular substructure of lamellar crystallites	1293
C. Zero-growth temperature	1294
D. Summary of controlling laws	1295
IV. Thermodynamics of Crystal Growth	1295
A. Applying Ostwald's rule of stages	1295
B. Multistage model and nanophase diagram	1296
C. Model-based data evaluation	1298
V. Final Remarks	1299
Acknowledgments	1299
References	1299

## I. INTRODUCTION

Considering that polymers are flexible long chains of coupled monomeric units, one might doubt at first whether such objects can crystallize at all. In fact, this is possible, but occurs in a peculiar way (Strobl, 2007). In principle, a periodic structure in three dimensions can be obtained by choosing a unique helical conformation for all chains, orienting the helix axes parallel to each other, and packing the chains in a regular manner. However, for obvious reasons such an ideal crystal structure is never found. Starting from the melt where the chains are coiled and penetrate each other, this ideal state cannot be reached; it would require a complete disentangling of all chains, which needs too long a time. About 50 years ago, electron micrographs like Fig. 1 were obtained, showing the natural structure of polymers; in this case, the surface of a solid sample of polyethylene (PE). The picture resembles a landscape with many terraces. It represents an oblique cut through stacks of lamellar, i.e., platelike, crystallites with curved edges. They have a lateral extension in the micrometer range and a thickness of about 20 nm. Figure 2 provides insight into the inner

\*strobl@uni-freiburg.de

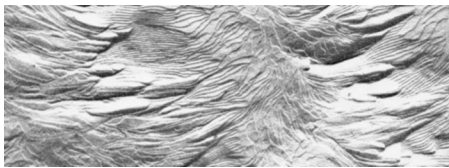


FIG. 1. Electron micrograph of a carbon film replica on a surface of PE (width of the depicted region is  $5\ \mu\text{m}$ ). One observes stacks of platelike crystallites with curved edges and a varying orientation on the sample surface. From [Eppe, Fischer, and Stuart, 1959](#).

structure of the stacks. It shows an electron micrograph obtained for an ultrathin slice of polyethylene which was stained with  $\text{OsO}_4$ . The staining agent is rejected by the crystallites and enters only regions that remain fluid. The contrast in the image then arises from the greater absorption of the electron beam in the stained (hence fluid) parts. The white lines depict lamellar crystallites, but only those that stand up, i.e., are oriented with their layer plane perpendicular to the slice surface; then the electron beam can pass through with minor absorption. The two micrographs are typical and exemplify the basic structural principle in the morphology of polymeric solids: These are built up as two-phase structures, and are composed of platelike crystallites that are separated by fluid regions. Cooling a melt to a temperature at which the polymer crystallizes results in a semicrystalline state with this character.

The development of such a structure is basically conceivable. Crystals of short-chain molecules such as the  $n$ -alkanes are also composed of stacks of layers, as is shown in Fig. 3. The interfaces are occupied by the end groups which cannot be incorporated in the interior parts of the layer. Similarly, polymer crystallization requires that one removes chain entanglements of the melt which cannot be resolved within the available short time. The entanglements are just shifted into the amorphous intercrystalline regions. Since the crystal thickness is small compared to the chain length, a given chain returns into the same or the adjacent crystal after an excursion into the amorphous region. For this reason the crystalline layers since their first discovery have been called “folded chain crystals.” Figure 4 depicts a section of such a polymer crystallite, showing its interior with

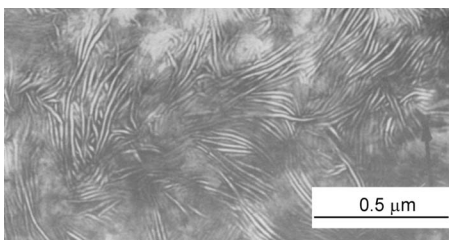


FIG. 2. Ultrathin slice of a PE sample stained with  $\text{OsO}_4$ . The bright lines are crystalline lamellae of PE which are oriented edge on, i.e., with the plate surface perpendicular to the surface of the slice. Crystallites are embedded in a dark fluid matrix. From [Kanig, 1975](#).

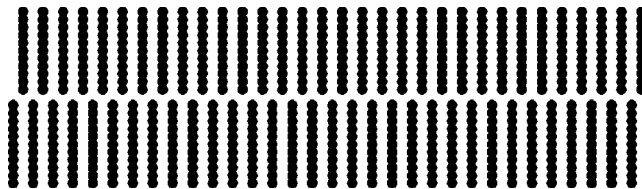


FIG. 3. Crystal structure of short-chain molecules like the  $n$ -alkanes. Schematic drawing with two layers. The layer thickness corresponds to the length of the molecules; the distance between neighbors is about  $0.5\ \text{nm}$ .

straight chain sequences and the two “fold surfaces.” The layer thickness depends on the crystallization temperature and generally increases with rising temperature.

When the crystallization process is followed in a polarizing optical microscope growing spherulites are often observed, as, for example, the sample of poly(L-lactide) (PLLA) shown in Fig. 5. The inner structure of these objects with sizes in the micrometer range is indicated in Fig. 6, together with an electron micrograph obtained for a spherulite of isotactic polystyrene (iPS). The structure results from a repeated branching and splaying of the crystal lamellae. This implies that the radial growth rate of a spherulite is identical with the lateral growth rate of the constituent lamellar crystallites. In fact, polymer crystals grow in the two lateral directions only—growth in the chain direction, i.e., normal to the plate surface, is blocked by the folds and loops. The growth rate varies with temperature in a peculiar manner, exemplified by poly( $\epsilon$ -caprolactone) (P $\epsilon$ CL) in Fig. 7: It decreases exponentially with rising temperature.

When these basic properties of crystallizing polymers were revealed in the 1950s, the search for understanding started immediately. Discussions first concerned the temperature-dependent selection of the lamellar crystallite thickness and the mechanism of lateral crystal growth. The debates were intense and a central topic in

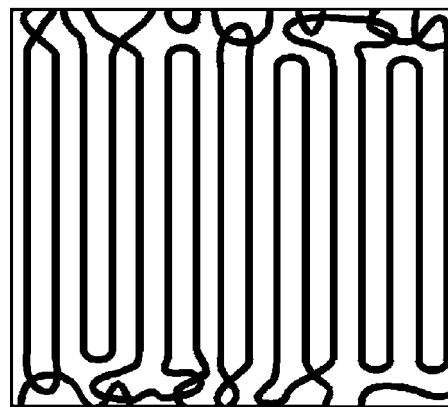


FIG. 4. Part of a lamellar crystallite in a semicrystalline polymer. Parallel straight chain sequences with a length of the order  $10\ \text{nm}$  set up the crystalline structure in the interior. The two surfaces, commonly called “fold surfaces,” are occupied by sharp folds, loops, entanglements, and other noncrystallizable chain parts.

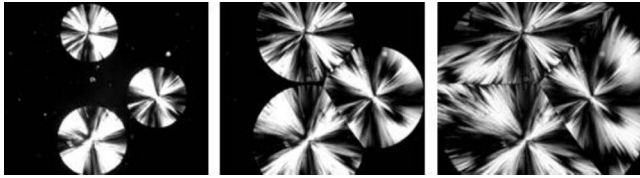


FIG. 5. Growing spherulites observed during the crystallization of PLLA in a polarizing optical microscope (width of depicted region is  $10\ \mu\text{m}$ ).

all structure-oriented conferences in the 1960s and 1970s. One conference, organized as a Faraday Discussion 1979 in Cambridge, became famous as a high point ([Faraday Discussion, 1979](#)). It brought together in often controversial discussions the different views and models developed by Fischer, Flory, Frank, Hoffman, Keller, Kovacs, Krimm, Point, Stein, and Wunderlich, to cite only some of many prominent contributors. An agreement between the scientists could not be reached, either at this conference or afterward. However, in the years that followed, one approach gained the ascendancy, and this was the one put forward by Hoffman, Lauritzen, and their co-workers ([Hoffman \*et al.\*, 1976](#)). It was accepted and used in data evaluations by more and more workers because the picture envisaged by the treatment was easy to grasp and the associated theory yielded simple equations for the lamellar thickness and the growth rate. The Hoffman-Lauritzen model was always accompanied by criticism, but this did not hinder its success. Some points were taken up and led to modifications, but the foundations remained unchanged. In the 1980s the model developed into the “standard model” of polymer crystallization and was broadly applied. The impression that the mechanism of polymer crystallization was understood in principle and the issue essentially settled was, however, wrong. With the 1990s revised thinking set in, triggered by new experimental results which contradicted the Hoffman-Lauritzen equations. It is now the common opinion that conventional wisdom is incorrect and needs revision. The experimental evidence is clear; the interpretation is under discussion. We offer

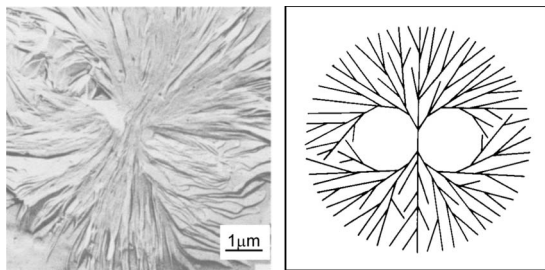


FIG. 6. Spherulite of iPS in an electron micrograph. The orientation of the lamellar crystallites varies. Those in the central parts of the lower half are standing up; those in the lower right corner are lying flat (left). Schematic drawing showing the inner structure of a spherulite resulting from branching and splaying (right). From [Vaughan and Bassett, 1989](#).

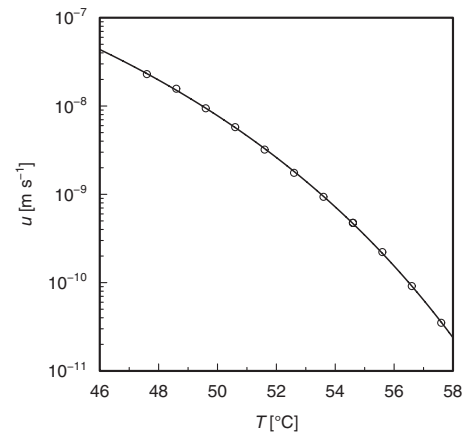


FIG. 7. Temperature dependence of the radial growth rate of spherulites of P $\epsilon$ CL. From [Cho \*et al.\*, 2007a](#).

a new approach to understanding polymer crystallization.

To justify once again the necessity of a change in understanding we begin with a description of the previous conventional views (Sec. II). Next the contradictory experimental results from the last decade are presented. They can be expressed by a set of laws which generally control crystallization and melting in polymeric systems (Sec. III). We understand these laws as clear indication of interference of a transient mesophase in the crystallization process and explain in the final section (Sec. IV) the proposed “multistage model.”

## II. CONVENTIONAL VIEWS: THE HOFFMAN-LAURITZEN MODEL

It is a characteristic property of polymer crystallization that growth rates vary exponentially with temperature, both near the melting point where they decay as demonstrated by the example of Fig. 7 and also near the glass transition where they increase with rising temperature (this temperature range is not included in the figure). The behavior indicates control of the growth process by some activation steps. Near the glass transition they occur related to the diffusive motion of chain sequences which have to pass over intramolecular and intermolecular activation barriers. Barrier heights are essentially constant so that the rates of jumps over the barriers increase with rising temperature. The conditions found in the high-temperature range near the melting point are different. The slowing down of growth when the temperature increases is indicative of an increase in the barrier height. The thickness of the lamellar crystallites generally increases when the crystallization temperature is increased. It was therefore an obvious idea to relate the two observations and to associate the increasing barrier height of the activation step with the increasing thickness of the growing crystallites. Hoffman and Lauritzen proposed the model sketched in Fig. 8. The drawing, reproduced from the original article, shows a lamellar crystallite which grows in one lateral direction only; the direction of growth is indicated by the vector

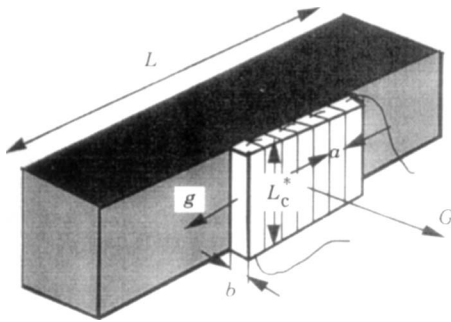


FIG. 8. Growth of a polymer crystallite as described by the Hoffman-Lauritzen model. The platelike crystallite (fold surface in dark color; the thickness here is denoted  $L_c^*$  and the width  $L$  is assumed constant) extends in one lateral direction only with a growth rate  $G$ . The rate-determining step is the formation of a secondary nucleus on the smooth growth face made up of refolded, repeatedly stretched chain sequences (folds connecting adjacent stems of stretched chain parts are indicated in the drawing). The attachment of further stems subsequent to the nucleation step (with rate  $g$ ) is treated as a rapid process ( $g \gg G$ ). From Hoffman, Davis, and Lauritzen, 1976.

$G$ . It is assumed that the growth face (with normal vector parallel to  $G$ ) is atomically smooth and that the rate-determining step is the formation of a secondary nucleus created by the attachment of a refolded, repeatedly stretched chain sequence from the melt onto the growth face. When the nucleus has formed it expands rapidly into a monomolecular layer. The model thus has many features of the layer-by-layer growth mode of low-molar-mass crystals, leading to a faceted shape. Based on this model Hoffman and Lauritzen analyzed the growth kinetics, looking for the crystal thickness which would give the maximum growth rate. In fact, the semicrystalline state does not represent a thermal equilibrium associated with the Gibbs free energy minimum, but is kinetically determined, i.e., the developing structure is that with the maximum rate of formation. The theoretical treatment resulted in the conclusion that the maximum growth rate is achieved by crystallites whose thickness is near the stability limit, i.e., the melting point, of the lamellar crystallites. The melting point of a crystal with thickness  $d_c$  (in Fig. 8 the thickness is denoted  $L_c^*$ ) is given by the Gibbs-Thomson equation as

$$T(d_c) = T_f^\infty - \frac{2\sigma_e T_f^\infty}{\Delta h_f} \frac{1}{d_c}. \quad (1)$$

Equation (1) describes the suppression of the melting point below the equilibrium value of a macroscopic body  $T_f^\infty$  caused by the excess free energy  $\sigma_e$  of the fold surface;  $\Delta h_f$  denotes the heat of fusion. For a crystallization temperature  $T$  the Hoffman-Lauritzen treatment predicted a thickness of the growing crystals of

$$d_c = 2\sigma_e T_f^\infty / \Delta h_f (T_f^\infty - T) + \delta; \quad (2)$$

hence, a value inversely proportional to the supercooling below  $T_f^\infty$ , apart from a minor excess  $\delta$  necessary for

providing a driving force. The associated growth rate  $u$  followed as

$$u = u_0 \exp\left(-\frac{T_A^*}{T}\right) \exp\left(-\frac{T_G}{T_f^\infty - T}\right). \quad (3)$$

The first exponential term expresses the temperature dependence of the segmental mobility in the melt; for temperatures far above the glass transition it obeys an Arrhenius law with some effective activation temperature  $T_A^*$ . The second exponential term refers to the free energy of activation associated with the placement of a secondary nucleus on the growth face. It diverges together with  $d_c$  at  $T_f^\infty$ . For the parameter  $T_G$  theory yielded an expression of the form

$$T_G = K/T, \quad (4)$$

with  $K$  determined by  $\Delta h_f$ ,  $\sigma_e$ , and the surface free energy  $\sigma_l$  of the growth face.

The Hoffman-Lauritzen model was widely accepted. It became a standard procedure to evaluate growth rate data of polymer systems as suggested by the theory, and to derive from the results the surface free energy of the secondary nucleus.

### III. NEW EXPERIMENTAL RESULTS

In the 1990s new ideas came up, triggered by new observations:

- Keller and his co-workers, when crystallizing polyethylene at elevated pressures, observed the formation of orthorhombic crystals out of a disordered hexagonal phase and speculated that this may also happen under normal pressure conditions (Rastogi *et al.*, 1991; Keller *et al.*, 1994).
- Kaji and co-workers interpreted a scattering of x rays which they observed prior to the scattering by crystallites as indicating the buildup of a precursor phase prior to the crystal formation (Imai *et al.*, 1995), and a corresponding theory was constructed by Olmsted *et al.* (1998).
- Temperature-dependent small-angle x-ray scattering (SAXS) experiments, first carried out for syndiotactic (*s*-)polypropylene (sPP) and related octene copolymers (sPPCo<sub>x</sub>; chains include a fraction  $x$  of statistically distributed octene co-units), contradicted the basic assumption of a control of the lamellar thickness by the supercooling below the equilibrium melting point (Hauser *et al.*, 1998).

#### A. Crystallization line, recrystallization line, and melting line

Considerations about mechanisms of crystallization and melting in polymers require as basic ingredients the following: knowledge of the variation in the crystal thickness  $d_c$  with the crystallization temperature, monitoring of possible structure changes during a heating to the melting point, and knowledge of the variation in the

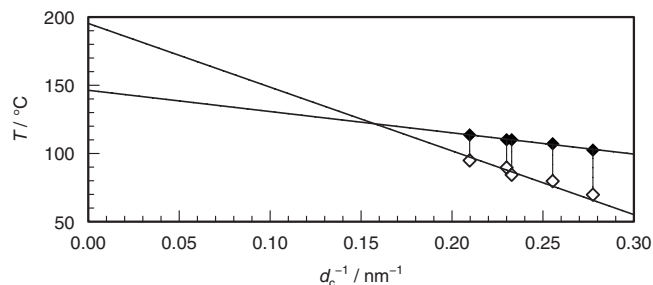


FIG. 9. sPPcO15: Results of temperature-dependent SAXS experiments. Crystallization line describing the relationship between the crystallization temperature  $T$  and the inverse crystal thickness  $d_c^{-1}$  (open symbols) and Gibbs-Thomson melting line giving the melting points  $T$  as a function of  $d_c^{-1}$  (filled symbols). The vertical direction of the connecting lines indicates that crystals have a constant thickness up to the melting point. From Hauser *et al.*, 1998.

melting temperature with the crystal thickness. During the development of the Hoffman-Lauritzen model, the focus was mainly on growth rate measurements; temperature-dependent studies of the lamellar structures were rare. With the aid of small-angle x-ray scattering experiments employing appropriate efficient methods of data evaluation (Ruland, 1977; Schmidtke *et al.*, 1997), it was possible to determine these structural properties, at first for *s*-polypropylene together with a variety of sPPcOs and then also for isotactic (*i*-)polypropylene (iPP), polyethylene together with octene copolymers (PEcO<sub>x</sub>), poly( $\epsilon$ -caprolactone), poly(L-lactide), and poly(1-butene) (Strobl, 2006). Figures 9 and 10 present as two typical examples the results obtained for sPPcO15 (*s*-polypropylene with 15% of octene units) and poly( $\epsilon$ -caprolactone). As suggested by the Gibbs-Thomson equation, the melting points are plotted as a function of the inverse crystal thickness  $d_c^{-1}$

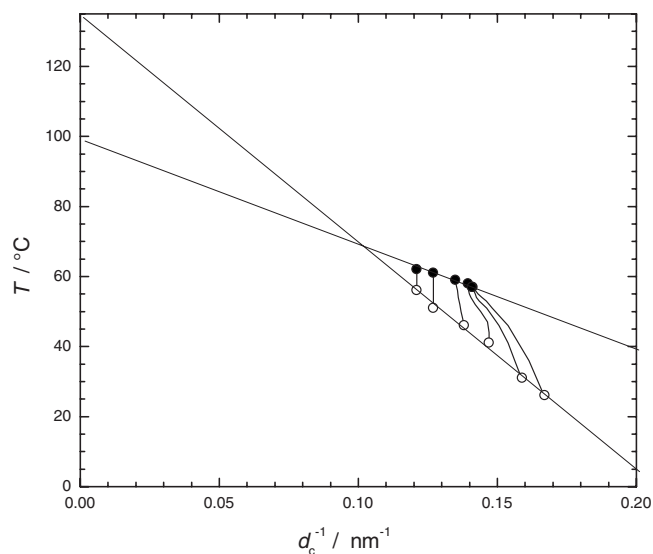


FIG. 10. P $\epsilon$ CL: Crystallization line and melting line. For crystallization temperatures below 40 °C crystals increase in thickness before the final melting. From Heck *et al.*, 1999.

and the same representation is also used here for the relation between the crystallization temperature and the crystal thickness. The appearance of the plots is peculiar and typical for all samples investigated: Two straight lines are found that cross each other. The “melting line,” giving the relation between the melting temperature and  $d_c^{-1}$  agrees with the Gibbs-Thomson equation. This allows determination of the equilibrium melting point  $T_f^\infty$  by a linear extrapolation to  $d_c^{-1}=0$ . The “crystallization line” gives the relationship between the crystallization temperature and  $d_c^{-1}$ . It has a higher slope than the melting line, intersects the latter at a finite value of  $d_c^{-1}$ , and has a limiting temperature for  $d_c^{-1}\rightarrow 0$ , denoted  $T_c^\infty$ , which differs from  $T_f^\infty$ . The crystallization line is described by

$$d_c^{-1} = C_c(T_c^\infty - T). \quad (5)$$

The crossing implies  $T_c^\infty > T_f^\infty$ . The results of the temperature-dependent measurements during heating are given by the thin lines which connect corresponding points on the crystallization and melting lines. The lines are vertical when the thickness remains constant and are curved when the thickness increases during heating.

The existence of straight crystallization lines in all systems investigated expresses a first simple law: Crystal thicknesses are inversely proportional to the distance from a certain characteristic temperature  $T_c^\infty$ , which is different from the equilibrium melting point  $T_f^\infty$ . In the two examples  $T_c^\infty$  is 35 and 50 °C above  $T_f^\infty$ .

Lamellar crystallites can exist only at temperatures below the melting line. Therefore, crystals with thicknesses as given by the crystallization line can no longer be formed when the temperature of the intersection point is approached. This is indeed experimentally confirmed. Results of small-angle x-ray scattering experiments in the temperature range for sPPcO20 are shown in Fig. 11. The points already deviate from the crystallization line before the point of intersection is reached. The results were obtained using a procedure known as “self-seeding,” which greatly enhances the number of nuclei and thus allows observation of crystallization processes at high temperatures also. The enhancement is achieved by stopping the heating process immediately after sample melting, followed by a rapid cooling down to the crystallization temperature.

The presence in a chain of co-units (units with a different chemical structure) which cannot be included in the crystal lattice modifies the crystallization and melting properties. Temperature-dependent small-angle x-ray scattering studies were carried out to see these effects. The findings for *s*-polypropylene and a variety of different sPPcOs are depicted in Fig. 12. In contrast to the normal behavior of the melting lines, which shift to lower temperatures when the co-unit content increases, the crystallization line is invariant within this set of samples. One observes a unique  $T$  vs  $d_c^{-1}$  relationship common to all of them, which determines  $d_c$  to be inversely proportional to the supercooling below  $T_c^\infty = 195$  °C.

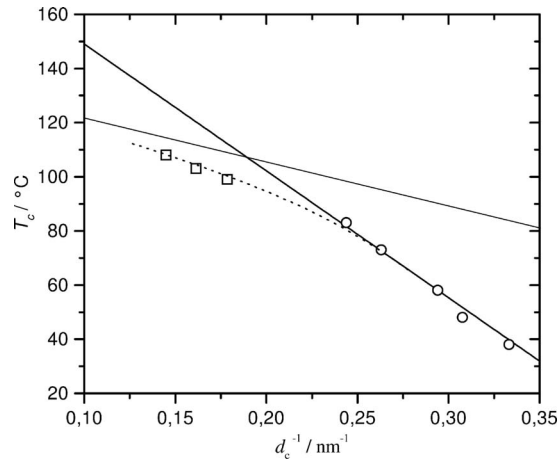


FIG. 11. sPPcO20: Relationship between crystallization temperature and crystal thickness in the range around the point of intersection between the melting and crystallization lines. Crystallization at the three highest temperatures (square symbols) was carried out by applying “self-seeding.” From Strobl, 2000.

For the crystallization temperatures chosen in the experiments of Fig. 12, all crystallites have constant thickness up to the point of melting. Different behavior is observed when the crystallization is carried out at lower temperatures, down to temperatures near the transition into the glassy state. When such a sample is heated after the completion of the crystallization, reorganization processes set in. The crystal thickness generally increases upon heating, and this reorganization process proceeds continuously. Figure 13 shows as an example the result of corresponding small-angle x-ray scattering experiments on three different samples of *s*-polypropylene. The samples were isothermally crystallized and then heated stepwise. The figures present the variation of the thickness up to the melting point, again in plots of  $d_c^{-1}$  versus the temperature. The initial points are located on

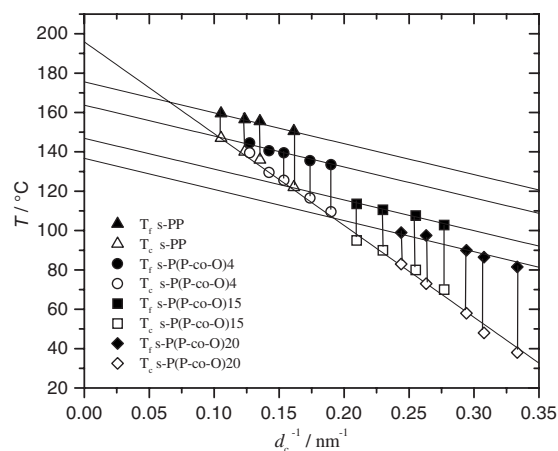


FIG. 12. sPP and sPPcOx: Unique crystallization line (open symbols) and series of melting lines (filled symbols). Extrapolation of the melting lines to  $d_c^{-1}=0$  yields the corresponding equilibrium melting points. They decrease with increasing co-unit content. From Hauser *et al.*, 1998.

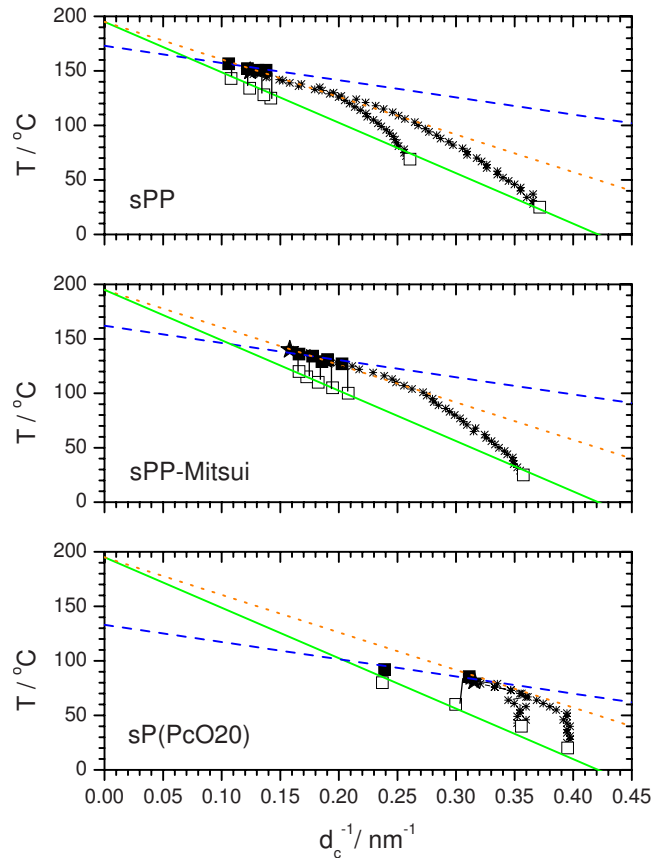


FIG. 13. (Color online) Three different samples of sPP, crystallized at various temperatures and heated: Inverse crystal thicknesses at the beginning (open squares), at melting points (filled squares), and at the end point of recrystallization processes (stars). All crystallization and recrystallization lines (dots) are identical, the melting lines (dashes) are shifted against each other. From Heck *et al.*, 2007.

the unique crystallization line of *s*-polypropylene. For crystallization temperatures in the low-temperature region, heating is accompanied by a continuous crystal thickening indicative of overall reorganization processes. Recrystallization goes on up to the temperature of final melting, indicated by a star. This temperature of final melting does not depend on the initial crystallization temperature. In the case of sPPcO20 crystallized at 20 °C, heating leaves the crystal thickness constant at first. This changes at 50 °C. Here thickening processes set in, and the further course is well defined:  $d_c^{-1}$  changes linearly with temperature following the drawn “recrystallization line.” Recrystallization ends at 85 °C with melting. The same dependence is observed when sP-PcO20 is at first crystallized at 40 °C. Recrystallization again sets in when the recrystallization line is reached, and  $d_c^{-1}$  follows this line from there on, up to the final melting. The line in the diagram guiding the process of recrystallization for sPPcO20 also controls the recrystallization for the other two samples. The line is included in Fig. 13. The recrystallization line has a characteristic property: Extrapolation of the line to  $d_c^{-1} \rightarrow 0$  ends at the same temperature as the crystallization line.

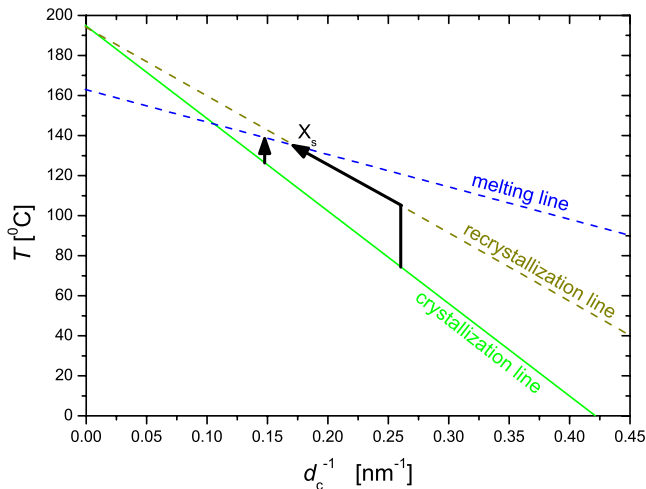


FIG. 14. (Color online) General scheme treating crystallization, recrystallization, and melting, exemplified with data of sPP. Sample-invariant crystallization and recrystallization lines; sample-dependent melting line (here for sPP-Mitsui). Pathways followed during heating processes subsequent to an isothermal crystallization at low temperatures (recrystallization before melting; fixed melting point  $X_s$  at the intersection of recrystallization line and melting line) and high temperatures (melting without prior recrystallization).

This recrystallization is a rapid process, much faster than the initial crystallization. This was demonstrated by Minakov *et al.* (2004) in a study of the melting of cold crystallized poly(ethylene terephthalate) with a chip calorimeter, which allows heating rates up to  $10^5 \text{ K min}^{-1}$  for thin films. Only for such high heating rates was recrystallization suppressed in this sample. On the other hand, for sufficiently low heating rates the structural changes are well defined and no longer rate dependent. A steplike sample heating with annealing times on the order of minutes is usually accompanied by full establishment of new stationary structures.

The results described suggest the validity of a simple scheme for the description of crystallization, recrystallization, and melting which can be generally applied to crystallizable polymers and related statistical copolymers. The scheme can be set up using a  $d_c^{-1}/T$  diagram and is presented in Fig. 14 using the data of one of the *s*-polypropylene samples. The diagram is composed of the following three lines: the crystallization line representing the relationship between the crystallization temperature and the inverse crystal thickness  $d_c^{-1}$ , the recrystallization line controlling the course of recrystallization processes, and the melting line with all final melting points. The crystallization and recrystallization lines are sample invariant, i.e., they are not affected by the co-unit content. The melting line, on the other hand, shifts to lower temperatures when the chemical disorder in the chain increases. The melting and recrystallization lines intersect each other at a certain temperature and a certain value of  $d_c^{-1}$ . This point of intersection, denoted  $X_s$  in Fig. 14, marks the end of the recrystallization processes. If the initial crystal thickness is greater than the

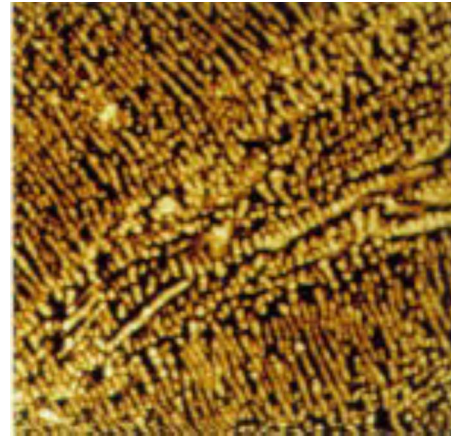


FIG. 15. (Color online) Sample of iPP: AFM tapping mode image of lamellar crystallites which stand up, i.e., are oriented with the fold surfaces perpendicular to the image plane. The lines representing the edges of the crystallites are not continuous as in the electron micrograph of Fig. 2 but broken up in small blocks. The image demonstrates that the lamellar crystallites have a granular substructure (scan over  $1 \mu\text{m}$  in both directions). From Magonov and Godovsky, 1999.

thickness at  $X_s$ , no recrystallization occurs; the sample just melts. For an initial thickness below the critical value, one always has recrystallization before melting. Whenever the recrystallization line is reached during a heating experiment,  $d_c^{-1}$  varies from there on linearly with  $T$ , guided by the line, up to the temperature at  $X_s$ , where the crystals melt. This temperature of final melting varies between different samples according to the position of  $X_s$ .

### B. Granular substructure of lamellar crystallites

The lamellar crystallites have a granular substructure. Evidence is provided by the widths of the  $hk0$  Bragg reflections in x-ray scattering patterns  $\Delta q_{hk0}$ , which are proportional to the inverse of the coherence length along the normal onto the respective lattice plane. Denoting the coherence length  $D_{hk0}$ , the relationship is described by the Scherrer equation

$$D_{hk0} = 2\pi/\Delta q_{hk0}. \quad (6)$$

For polymers, reflections are much broader than in the case of low-molar-mass crystals and generally indicate coherence lengths of several to some tens of nanometers. This small coherence length is to be identified with the extension of the crystal blocks which compose the lamella. They show up directly in electron micrographs, then, when a staining agent penetrates into the block boundaries (Michler, 1992), and sometimes in atomic force microscope (AFM) images. The examples presented in Figs. 15 and 16 were obtained for samples of *i*-polypropylene and *s*-polypropylene, respectively. The granular structure is clearly apparent, and, as we see, the lateral extension of the blocks is comparable to the crystallite thickness.

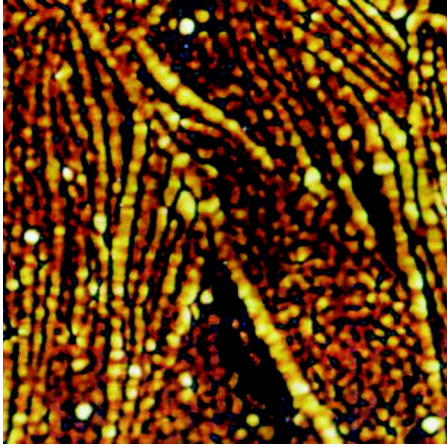


FIG. 16. (Color online) Sample of sPP: AFM tapping mode image of the edges of up standing crystals showing a granular substructure (scan over  $1.25 \mu\text{m}$  in both directions). From [Hugel et al., 1999](#).

It turns out that the lateral size of the blocks changes with temperature in a systematic manner, namely, exactly proportionally to the crystal thickness  $d_c$ . Figure 17 presents the temperature dependence of the two lengths  $d_c$  and  $D_{200}$  as obtained for different samples of *s*-polypropylene. As can be seen, all points  $D_{200}^{-1}(T)$  fall on one common line. When continued, this line ends again at  $T_c^\infty = 195^\circ\text{C}$ , like the crystallization line of *s*-polypropylene. Analogous results were obtained for polyethylene and related copolymers ([Hippler et al., 2005](#)).

### C. Zero-growth temperature

For many decades it was taken for granted that the growth rate of polymer crystallites is controlled by supercooling below the equilibrium melting point of a

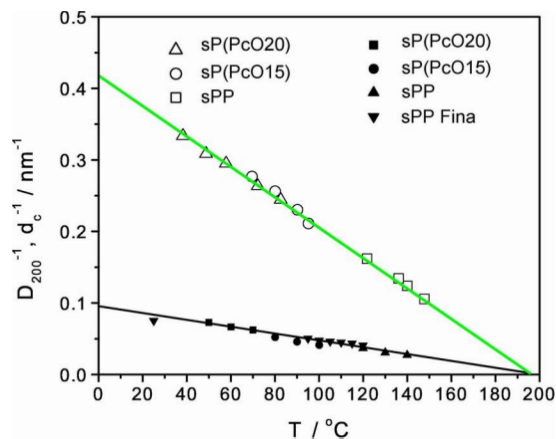


FIG. 17. (Color online) Different samples of sPP (sPP, sPPcOx, and sPP-Fina) crystallized at various temperatures  $T$ : Crystallization line  $d_c^{-1}$  vs  $T$  determined by SAXS (open symbols) and inverse lateral coherence lengths  $D_{200}^{-1}$  derived from the line-width of the 200 reflection (filled symbols). From [Hippler et al., 2005](#).

macroscopic sample  $T_f^\infty$ , and Eq. (3) of the Hoffman-Lauritzen model was generally used in evaluations of temperature-dependent growth rate measurements. Growth rates are controlled by an activation barrier, and the second exponential factor in Eq. (3) states that the height of this activation barrier diverges at  $T_f^\infty$ . In the Hoffman-Lauritzen model this is a consequence of the divergence of both the crystal thickness and the size of the secondary nucleus at  $T_f^\infty$ , as described by Eq. (2). The small-angle x-ray scattering experiments described in Sec. III.A contradict Eq. (2); the temperature dependence of the crystal thickness is given by Eq. (5), which no longer includes  $T_f^\infty$ . As a consequence, doubts arose also with regard to the validity of Eq. (3).

In a first check we carried out growth rate measurements on poly( $\epsilon$ -caprolactone). Its crystallization and melting properties were well characterized by small-angle x-ray scattering experiments. The equilibrium melting point is  $T_f^\infty = 99^\circ\text{C}$ , and the temperature controlling the crystal thickness according to Eq. (5) is  $T_c^\infty = 135^\circ\text{C}$  (see Fig. 10). The difference between these two temperatures is especially large. In poly( $\epsilon$ -caprolactone), a small number of spherulites is slowly growing to large sizes, which is a favorable situation for accurate growth rate measurements in a polarizing optical microscope. The results were already presented, in Fig. 7, giving growth rates between  $47$  and  $58^\circ\text{C}$ .

Equation (3) includes as a basic assumption that the activation energy diverges at  $T_f^\infty$ . The correctness of this assumption can be examined by the experiment. One replaces the set parameter  $T_f^\infty$  by a variable temperature  $T_{zg}$ . Differentiation of  $\ln u$  with regard to  $T$  and some reordering leads to

$$\left( -\frac{d \ln(u/u_0)}{dT} + \frac{T_A^*}{T^2} \right)^{-1/2} = T_G^{-1/2} (T_{zg} - T). \quad (7)$$

Application of this equation allows  $T_{zg}$  to be determined; values for  $T_A^*$  are available in the literature. Figure 18 presents a plot as suggested by Eq. (7). As is obvious, the equation can be used for a determination of the “zero-growth temperature”  $T_{zg}$ . The data points all lie on a straight line, and extrapolation down to zero yields  $T_{zg}$  with a value of  $77^\circ\text{C}$ . This temperature is far below the equilibrium melting point of  $99^\circ\text{C}$ .

A second check concerned the growth rate of polyethylene. Here the equilibrium melting point is located between  $141.4^\circ\text{C}$  [given by Wunderlich as measured for macroscopic “extended chain crystals” ([Wunderlich, 1980](#))] and  $144.7^\circ\text{C}$  [derived by Flory and Vrij using an extrapolation of *n*-alkane melting points ([Flory and Vrij, 1963](#))]. Figure 19 shows data for measurements plotted as suggested by Eq. (7). The result for  $T_{zg}$  is  $132.6^\circ\text{C}$ , which is again far below the equilibrium melting point.

Hence, the broadly used Eq. (3), is indeed incorrect. The activation energy does not diverge at  $T_f^\infty$  but definitely earlier. Obviously Eq. (3) has to be replaced by another relationship, namely,

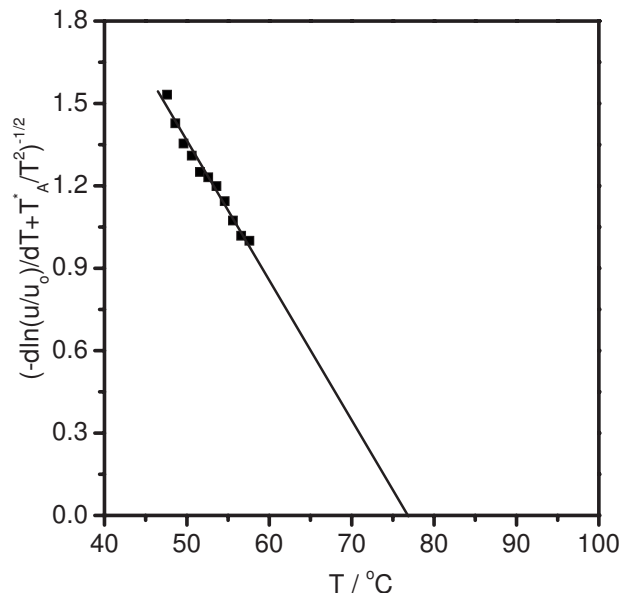


FIG. 18. PεCL: Temperature dependence of the radial growth rate. Plot based on Eq. (7) giving  $T_{zg}=77$  °C. From Cho *et al.*, 2007a.

$$u = u_0 \exp\left(-\frac{T_A^*}{T}\right) \exp\left(-\frac{T_G}{T_{zg} - T}\right). \quad (8)$$

This equation includes  $T_{zg}$  as a third temperature characteristic for a given polymer system, different from both  $T_f^\infty$  and  $T_c^\infty$ .

#### D. Summary of controlling laws

Thus, as we have seen, experiments have revealed that the crystallization and melting of polymers in bulk can be described by a number of laws. We summarize them again here as follows:

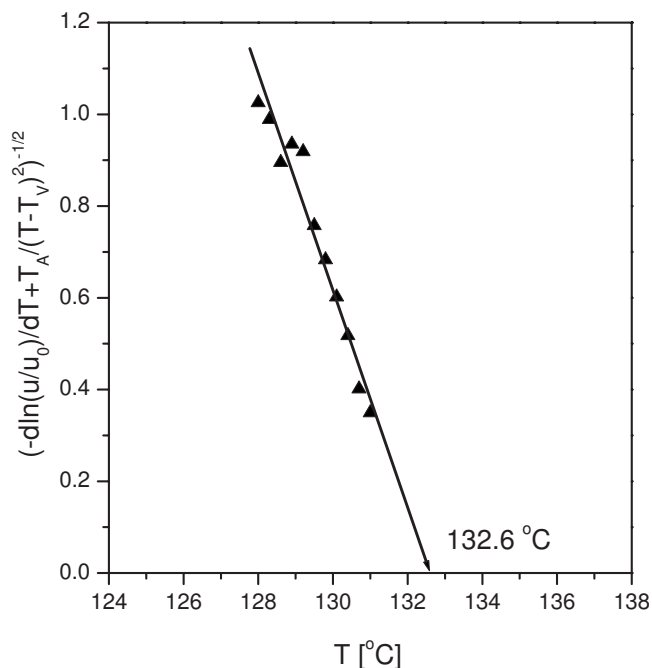


FIG. 19. Growth rates of PE represented according to Eq. (7). From Cho *et al.*, 2007b.

- The first law gives the melting point  $T$  of platelike crystallites with thickness  $d_c$  which is depressed due to the excess free energy of the fold surface. It is expressed by the Gibbs-Thomson equation (1),

$$d_c^{-1} = C_f(T_f^\infty - T) \quad \text{with } C_f = \Delta h_f / 2\sigma_e T_f^\infty.$$

$T_f^\infty$  is the equilibrium melting point of macroscopic crystals. If co-units are incorporated in the chains, a further drop of melting points results.

- A second law concerns the relationship between the crystal thickness and the crystallization temperature  $T$ . It also has the form of a Gibbs-Thomson equation, but includes another controlling temperature  $T_c^\infty$  [Eq. (5)],

$$d_c^{-1} = C_c(T_c^\infty - T).$$

Equation (5) is an important property, holding commonly for the homopolymer and related statistical copolymers of a system.

- For crystallization temperatures below some characteristic value, subsequent heating leads to continuous recrystallization processes. They follow the recrystallization line given by

$$d_c^{-1} = C_r(T_c^\infty - T). \quad (9)$$

All recrystallized samples melt at the same point, independent of the initial crystallization temperature.

- A further law concerns the temperature dependence of the lateral size of the crystalline blocks which are the constituent elements of the lamellae: The lateral extension of the blocks is proportional to their height in the chain direction  $d_c$ .
- Crystallites grow in the lateral direction only, with a rate that increases exponentially with the supercooling below the zero growth temperature  $T_{zg}$  as expressed by Eq. (8).

Polymer crystallization and melting processes are thus controlled by three characteristic temperatures,  $T_f^\infty$ ,  $T_c^\infty$ , and  $T_{zg}$ . They are arranged as

$$T_{zg} < T_f^\infty < T_c^\infty.$$

## IV. THERMODYNAMICS OF CRYSTAL GROWTH

### A. Applying Ostwald's rule of stages

Given this set of experimentally well-founded laws one has to ask about their physical background. What is the reason for the occurrence of three characteristic controlling temperatures? What is the meaning of the various lines showing up in a  $T/d_c^{-1}$  diagram? To begin with, the difference between the crystallization and melting lines in the macroscopic limiting temperature and the effect of co-units demonstrates that different laws control crystallization and melting in bulk polymers. Here crystallization and melting are not reverse processes. While melting is certainly associated with a direct trans-

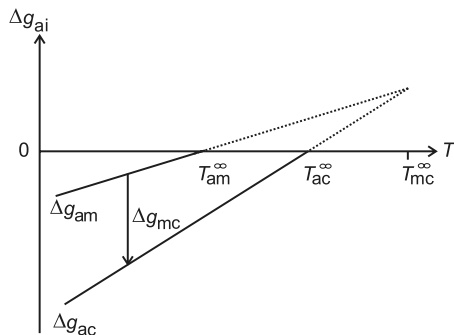


FIG. 20. Thermodynamic conditions assumed for crystallizing polymers: Temperature dependencies of the bulk chemical potentials of a mesomorphous (label *m*) and the crystalline phase (*c*). The potentials are referred to the chemical potential of the amorphous melt (*a*). From Strobl, 2006.

fer of chain sequences from lateral crystal faces into the melt, formation of crystals follows another route—very probably one that uses a passage through some intermediate phase. In their crystallization experiments on polyethylene at elevated pressures during the early 1990s, Keller and co-workers observed a nucleation into a metastable hexagonal phase prior to the transformation into the stable orthorhombic phase (Rastogi *et al.*, 1991; Keller *et al.*, 1994). They interpreted their observations as an example for Ostwald’s rule of stages. This rule, formulated about one hundred years earlier, states that crystals nucleate into that mesomorphous or crystalline structure which is the most stable one for nanometer-sized objects (Ostwald, 1897). Due to differences in the surface free energy, this state may differ from the macroscopically stable crystal form. In searching for an understanding of polymer crystallization under normal pressure conditions, we felt that Ostwald’s rule of stages when applied to the growth process might again provide the clue, and developed a corresponding model.

Indeed, participation of a transient “mesophase” with a state of order intermediate between the melt and the crystal yields a natural explanation for the existence of three controlling temperatures. These can be identified with the three transition temperatures between the melt, the crystal, and the mesophase. The basic conditions under which such a mesomorphous phase can interfere and thus affect the crystallization process are described in Fig. 20. The scheme shows for both the crystalline and mesomorphous phases the difference of the bulk chemical potential from that of the melt,

$$\Delta g_{ac} = g_c - g_a, \quad \Delta g_{am} = g_m - g_a. \quad (10)$$

Coming from high temperatures, the chemical potential of the crystalline phase drops below the value of the melt when the equilibrium melting point  $T_{ac}^{\infty}$  is crossed. The mesomorphous phase requires a lower temperature to fall with its chemical potential below that of the melt, here named  $T_{am}^{\infty}$ . The plot also includes the temperature  $T_{mc}^{\infty}$ ; it represents the temperature of a virtual transition, namely, that between the mesomorphous and the crystalline phase. The three temperatures have the order

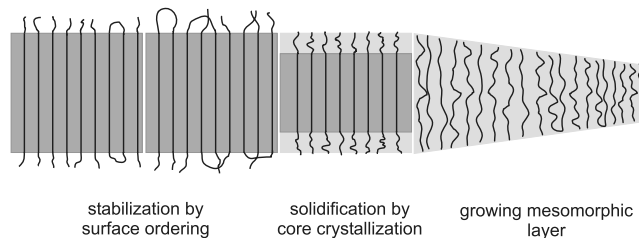


FIG. 21. Multistage model of polymer crystal growth. Rather than directly attached to the crystal surface, chain segments of the melt are first incorporated in a thin layer with mesomorphous structure in front of the crystallite. The mesomorphous layer thickens spontaneously. When a critical thickness is reached, a crystal block forms by a first-order transition. In the last step the excess energy of the fold surface is reduced. From Strobl, 2007.

$$T_{am}^{\infty} < T_{ac}^{\infty} < T_{mc}^{\infty}. \quad (11)$$

Since the bulk chemical potential of the crystal is always below that of the mesomorphous phase, the mesomorphous phase is metastable only for macroscopic systems. However, for small objects, with sizes in the nanometer range, the stabilities can be inverted. Because of their usually lower surface free energy, thin mesomorphous layers can have a lower Gibbs free energy than a crystallite with the same thickness. Then Ostwald’s rule of stages applies.

Thermodynamics relates the three transition temperatures  $T_{am}^{\infty}$ ,  $T_{ac}^{\infty}$ , and  $T_{mc}^{\infty}$  to the entropy increases  $\Delta s_{ma} = s_a - s_m$  and  $\Delta s_{ca} = s_a - s_c$  associated with melting of the mesomorphous and crystalline phases, respectively. Since the slopes of  $\Delta g_{am}$  and  $\Delta g_{ac}$  are given by  $\Delta s_{ma}$  and  $\Delta s_{ca}$ , one can write in linear approximation

$$(T_{mc}^{\infty} - T_{ac}^{\infty})\Delta s_{ca} \approx (T_{mc}^{\infty} - T_{am}^{\infty})\Delta s_{ma} \quad (12)$$

or

$$\frac{\Delta h_{ma}}{\Delta h_{ca}} = \frac{\Delta s_{ma} T_{am}^{\infty}}{\Delta s_{ca} T_{ac}^{\infty}} \approx \frac{(T_{mc}^{\infty} - T_{ac}^{\infty}) T_{am}^{\infty}}{(T_{mc}^{\infty} - T_{am}^{\infty}) T_{ac}^{\infty}}. \quad (13)$$

## B. Multistage model and nanophase diagram

A possible pathway for the growth of polymer crystallites mediated by a mesophase is shown in Fig. 21. In this multistage model, crystal growth proceeds in several steps. A thin layer with mesomorphous inner structure forms between the lateral crystal face and the melt, stabilized by epitaxial forces. All the co-units are already rejected on its front. A high inner mobility allows spontaneous thickening of the layer up to a critical value where the core region crystallizes with formation of a block. In the last step the surface region of this block, at first still disordered, perfects, which leads to a further stabilization. Based on this model it is possible to construct a thermodynamic scheme which shows all the features of Fig. 14, i.e., a crystallization line, a recrystallization line, and a melting line. It deals with four different phases: the melt, mesomorphous layers, and two limiting

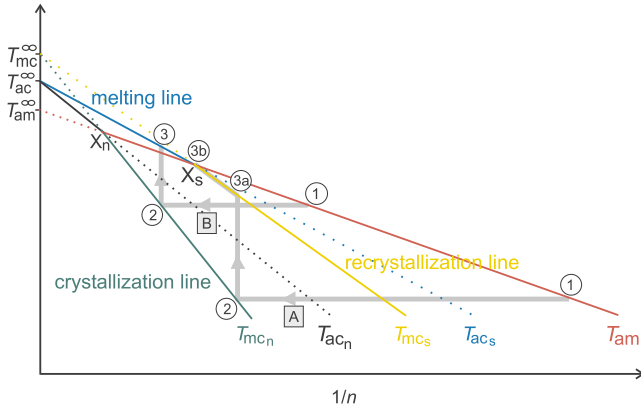


FIG. 22. (Color online)  $T/n^{-1}$  phase diagram for polymer layers in a melt (label *a*) dealing with three phases: mesomorphic (*m*), native crystalline (*c<sub>n</sub>*), and stabilized crystalline (*c<sub>s</sub>*). Lines of size-dependent phase transitions:  $T_{mc_n}$  between mesomorphic and native crystalline layers,  $T_{ac_n}$ ,  $T_{mc_s}$ ,  $T_{ac_s}$ , and  $T_{am}$  with corresponding meanings. Two routes for an isothermal crystallization followed by heating: route A for low crystallization temperatures and route B for high crystallization temperatures. Triple points  $X_n$  ( $X_s$ ) with coinciding Gibbs free energies of the melt, a mesomorphic layer, and a native (stabilized) crystalline layer with the same thickness. From Strobl, 2006.

forms of the crystallites, namely, native crystals (labeled  $c_n$ ) and stabilized crystals (with label  $c_s$ ). The scheme displayed in Fig. 22 delineates the stability ranges and transition lines for these phases. The variables in this phase diagram are the same ones as in Fig. 14, i.e., the temperature and the inverse crystal thickness, the latter being given by the number  $n$  of structure units in a stem,  $n = d_c / \Delta z$  with  $\Delta z$  the length per structure unit. Application of the model implies that the three lines in Fig. 14 can be interpreted as transition lines in a  $T/d_c^{-1}$  phase diagram, identifying the line named  $T_{ac_s}$  with the melting line ( $T_{ac} = T_f$ ), the line  $T_{mc_n}$  with the crystallization line, which implies in particular that  $T_c$ , the controlling temperature for the crystal thickness, is set equal to the transition temperature  $T_{mc}$ , and the line  $T_{mc_s}$  with the recrystallization line. The Gibbs-Thomson equation generally deals with the effect of surface free energies on transition temperatures. It can be applied not only to lamellar crystallites but in an analogous manner also to temperature- and size-dependent transitions of layers with mesomorphic structure. This leads for the crystallization line to the theoretical expression

$$T_c^\infty - T \approx \frac{(2\sigma_{ac_n} - 2\sigma_{am})T_c^\infty}{\Delta h_{cm}} \frac{1}{n} \quad (14)$$

and for the recrystallization line to

$$T_c^\infty - T \approx \frac{(2\sigma_{ac_s} - 2\sigma_{am})T_c^\infty}{\Delta h_{cm}} \frac{1}{n}. \quad (15)$$

$\sigma_{am}$  and  $\sigma_{ac_n}$  denote the surface free energy of the mesomorphic layer and the native crystal layer, respectively. The surface free energy of the stabilized crystallites, denoted  $\sigma_e$  in Eq. (1), is renamed as  $\sigma_{ac_s}$ .

The thermodynamic scheme associated with the model includes as a further line the stability limit  $T_{am}$  of layers with mesomorphic structure, which starts from the macroscopic transition temperature  $T_{am}^\infty$ . The Gibbs-Thomson equation yields for this case

$$T_{am}^\infty - T \approx \frac{2\sigma_{am}T_{am}^\infty}{\Delta h_{ma}} \frac{1}{n}. \quad (16)$$

For temperatures above  $T_{am}^\infty$  the mesophase no longer exists. The mesophase-mediated growth process assumed by the multistage model here comes to an end. This, however, is exactly the property of the zero-growth temperature. Hence, we identify  $T_{zg}$  with  $T_{am}^\infty$ . Note that the ordering of the limiting temperatures in the model [Eq. (11)] agrees with the observations

$$T_{zg} = T_{am}^\infty < T_f^\infty = T_{ac}^\infty < T_c^\infty = T_{mc}^\infty.$$

Of particular importance in the “nanophase diagram” of Fig. 22 are the triple points  $X_n$  and  $X_s$ . At  $X_n$  both mesomorphic layers and native crystals have the same Gibbs free energy as the melt; at  $X_s$  this equality holds for the stabilized crystallites. The positions of  $X_n$  and  $X_s$  control what happens during an isothermal crystallization followed by heating. In agreement with the experiments, the scheme predicts two different scenarios exemplified by the routes A and B. Route B, realized by crystallization at high temperatures, is as follows: At the point of entry, labeled 1, chains are attached from the melt onto the front of a mesomorphic layer with minimum thickness. The layer spontaneously thickens until the transition line  $T_{mc_n}$  is reached at point 2, where native crystals form immediately. The subsequent stabilization transforms them into a lower free energy state, and the crossing point is shifted to  $X_s$ . On heating, the crystallites remain stable up to the transition line  $T_{ac_s}$  associated with melting of the crystal. Route A (low crystallization temperatures) is different: The beginning is the same—starting at point 1 with attachment of chain sequences onto a spontaneously thickening mesomorphic layer, and then, on reaching  $T_{mc_n}$ , the formation of native crystals followed by stabilization. When the stabilized crystals are heated, they at first retain their structure. However, now the transition line  $T_{mc_s}$  is first met; this relates to a transformation into the mesomorphic state instead of melting. The consequence for further heating is a continuous recrystallization mediated by the mesophase (points 3a to 3b). This ends at the triple point  $X_s$  where the crystal melts.

What is the nature of the temperature-dependent activation barrier that shows up in the second exponential factor in Eq. (8) and determines the growth rate? The proposed multistage model includes a possible answer. The series of steps in Fig. 21 involves several activation barriers. The first step—attachment of a chain sequence on the growth front of the mesomorphic layer—could be dominant, and the observations support this supposition. Before a sequence, which lies coiled in the melt, is incorporated into the growing mesomorphic layer, it has to be “activated” by a transfer into an overall straightened

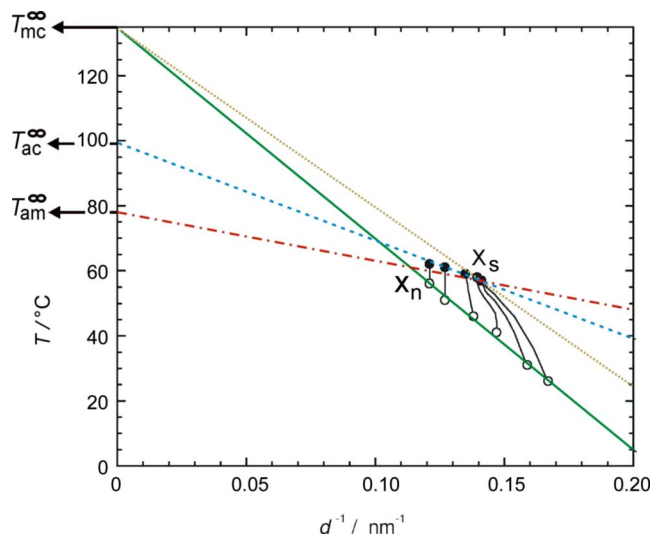


FIG. 23. (Color online) P $\epsilon$ CL: Crystallization line (continuous), recrystallization line (dots), and melting line (dashes) determined by SAXS, zero-growth-rate temperature  $T_{am}^\infty$  (from Fig. 18), and  $a \Rightarrow m$  transition line passing through  $T_{am}^\infty$  and  $X_s$  (dash-dotted line). From Strobl, 2007.

form as required for attachment. The straightening has to reach at least the length given by the initial thickness of the mesomorphic layer. The number of monomers in such a sequence  $n^*$  is determined by Eq. (16) as

$$n^* = \frac{2\sigma_{am}T_{am}^\infty}{\Delta h_{ma}} \frac{1}{T_{am}^\infty - T}. \quad (17)$$

Since the straightening leads to a decrease in entropy which is proportional to the sequence length it introduces an entropic activation barrier

$$-\Delta S/k \propto n^*. \quad (18)$$

Transition of the barrier takes place with a probability

$$\exp\left(\frac{\Delta S}{k}\right) = \exp\left(-\frac{\text{const}}{T_{am}^\infty - T}\right). \quad (19)$$

Since we identify  $T_{am}^\infty$  with  $T_{zg}$ , the theoretical expression agrees with the experimental result as given by Eq. (8).

### C. Model-based data evaluation

Application of the scheme to experimental results, as given by the crystallization line, the melting line, the

recrystallization line of a system, and the zero-growth-rate temperature, yields the thermodynamic parameters included in the equilibrium relationships. Figure 23 shows the data of poly( $\epsilon$ -caprolactone) from Fig. 10, now complemented by the recrystallization line and the  $a \Rightarrow m$  transition line. The latter is fixed by  $T_{am}^\infty$  ( $=T_{zg}$ ) and the location of  $X_s$ .

Evaluation of such a nanophase diagram yields the enthalpy change  $\Delta h_{ma}$  between the mesomorphic and amorphous phases, the surface free energy of mesomorphic lamellae  $\sigma_{am}$ , the surface free energy of crystalline lamellae in the initial native state  $\sigma_{ac_s}$ , and the surface free energy of crystalline lamellae in the final stabilized state  $\sigma_{ac_n}$ . The heat of fusion  $\Delta h_{ca}$  is usually available in the literature or can be determined by calorimetry. The heat of transition  $\Delta h_{ma}$  then follows from application of Eq. (13). In the next step  $\sigma_{am}$  is calculated using Eq. (16). The surface free energy  $\sigma_{ac_n}$  is obtained using Eq. (14) with  $\Delta h_{cm} = \Delta h_{ca} - \Delta h_{ma}$ . The surface free energy of the stabilized crystallites can be calculated by applying the corresponding relation Eq. (15).

The data derived in this way for poly( $\epsilon$ -caprolactone) from the nanophase diagram in Fig. 23 are collected in Table I.

The heat of transition  $\Delta h_{ma}$  is indicative of a truly intermediate character of the mesomorphic phase, which is neither nearly liquid nor resembles a perturbed crystallite. Comparing mesomorphic with crystalline lamellae, the drop of the surface free energy, from  $\sigma_{ac_n}$  and  $\sigma_{ac_s}$  to  $\sigma_{am}$ , is larger than that in the heat of transition from  $\Delta h_{ca}$  to  $\Delta h_{ma}$ . This is, indeed, an expected result. Only under this condition do the stabilities of crystalline and mesomorphic lamellae become inverted for nanocrystallites, thus opening the mesophase-mediated growth route.

With the  $a \Rightarrow m$  transition line the triple point  $X_n$  is also fixed, located at the intersection with the crystallization line. The point  $X_n$  marks the end of the mesophase-mediated growth process. For crystallization temperatures above  $T(X_n)$  and crystal thicknesses above  $d(X_n)$ , growth must proceed by direct attachment of chain sequences onto the lateral growth face of the crystal. It appears that so far experiments have not entered this temperature range. In principle, polymers also crystallize between  $T(X_n)$  and  $T_{ac}$ ; however, this apparently occurs with a vanishingly low rate. For the observed crystallization rates, the participation of an intermediate mesomorphic phase is obviously a necessity.

TABLE I. P $\epsilon$ CL: Thermodynamic data derived from the experiments.

$T_{mc}^\infty$ (°C)	$T_{ac}^\infty$ (°C)	$T_{am}^\infty$ (°C)	$\Delta h_{ca}$ ( $\frac{\text{kJ}}{\text{mol C}_6\text{H}_{10}\text{O}_2}$ )	$\Delta h_{ma}$ ( $\frac{\text{kJ}}{\text{mol C}_6\text{H}_{10}\text{O}_2}$ )	$\sigma_{ac_n}$ ( $\frac{\text{kJ}}{\text{mol}}$ )	$\sigma_{ac_s}$ ( $\frac{\text{kJ}}{\text{mol}}$ )	$\sigma_{am}$ ( $\frac{\text{kJ}}{\text{mol}}$ )
135	99	78	17.9	11.4	9.7	8.4	2.5

## V. FINAL REMARKS

In the field of polymer crystallization we are presently in a time of paradigm shifting away from conventional wisdom, but more time will be needed to establish a generally accepted new understanding. The experimental results presented provide a sound basis. They can be expressed by some equations of simple form which relate the thickness and growth rate of the platelike crystallites in polymeric solids to the supercooling below two characteristic temperatures. Since both differ from the equilibrium melting point, their existence invalidates the long-accepted Hoffman-Lauritzen model. The findings, resulting from temperature-dependent structural studies using x-ray scattering and optical microscopy, require a comprehensive explanation. The existence of three different controlling temperatures rather than a unique one is indicative of the participation of a third transient phase in the growth process, and we developed a corresponding theoretical model on thermodynamics grounds. The response in the polymer physics community varies; we do not see a blunt rejection but full acceptance is also rare. Of course, we hope that our view finally will be accepted as the correct concept, but are aware that this has not yet occurred. The whole community would be much more readily convinced if the proposed presence of a small region with mesomorphic structure at the front of a growing lamellar crystallite could be shown directly, rather than being inferred from the laws that govern crystallization and melting. Atomic force microscopy (AFM) with its high spatial resolution has the potential to realize this aim; however, so far an image with the character of the multistage model in Fig. 21 has not been reported. The reason could be that the mesomorphic phase is passed through very rapidly, maybe so rapidly that it exists as a transient state only during the formation of a block. The block formation would then resemble the formation of a nucleus, and the building of a crystal lamella consequently a repeated self-supported and guided nucleation. That crystal nucleation can be accelerated by passage through an intermediate phase has been known since Ostwald's time, and it is corroborated by convincing experiments, for example, by the nucleation studies on *n*-alkanes carried out by Sirota and Herhold (1999). There could, however, also be another reason for the nonvisibility of the mesomorphic phase in the AFM studies: Its surface stiffness could be close to that of the crystal so that the contrast would be insufficient to show up in the images. Li *et al.* (2001) reported a certain weakness of the front zone of growing polyester lamellae and related it to perturbations of the crystal structure.

The necessary revision of the traditional views about the crystallization in bulk polymer melts has revived the debate after a long period with reduced interest. There are several further issues, new and traditional ones, some of them of great technical importance, which are now intensely discussed at general conferences and focused meetings [see, for example, the report of the last EPS Discussion Meeting in Waldau (Reiter and Strobl,

2007)]. These are, in particular, primary nucleation phenomena, long-living structures in the melt that affect the crystallization process, confinement effects on crystallization as they are found, for example, in block copolymers, crystallization in flowing melts with oriented chains, and mobility restrictions in the regions near crystallites. Conditions in polymeric systems are peculiar and different from those in other materials. Experiments on polymeric systems therefore always require special tools for the preparation or the data evaluation and specific approaches have to be used in theoretical treatments or computer simulations. For a long period, polymer physics played only a side role in teaching and research programs of physics departments, if it was included at all. With the development of biophysics, organic electronics, and the various uses of soft matter, the situation has changed. Polymer physics provides the basis, and polymer crystallization is here a central phenomenon.

## ACKNOWLEDGMENTS

This work was carried out in Freiburg during the last decade by technicians, students, and postdocs of my group—Mahmud Al-Hussein, Simon Armbruster, Tai-Yon Cho, Jens Fritsch, Qiang Fu, Michael Grasruck, Andreas Häfele, Georg Hauser, Barbara Heck, Christoph Hertlein, Thomas Hippler, Wenbing Hu, Torsten Hugel, Masanori Iijima, Takahiko Kawai, Simon Keller, Peter Kohn, Eduard Sadiku, Jürgen Schmidtke, Sylvia Siegenführ, Werner Stille, and Thomas Thurn-Albrecht and I express here my high appreciation for their most engaged, successful work. We are also very grateful for the support of our activities by the “Deutsche Forschungsgemeinschaft” and by the “Fonds der Chemischen Industrie.”

## REFERENCES

- Cho, T., W. Stille, and G. Strobl, 2007a, *Colloid Polym. Sci.* **285**, 931.
- Cho, T., W. Stille, and G. Strobl, 2007b, *Macromolecules* **40**, 2590.
- Eppe, R., E. Fischer, and H. Stuart, 1959, *J. Polym. Sci.* **34**, 721.
- Faraday-Discussion, *Organization of Macromolecules in the Condensed Phase*, 1979, Faraday Discuss. Chem. Soc. **85**.
- Flory, P., and A. Vrij, 1963, *J. Am. Chem. Soc.* **85**, 3548.
- Hauser, G., J. Schmidtke, and G. Strobl, 1998, *Macromolecules* **31**, 6250.
- Heck, B., T. Hugel, M. Iijima, E. Sadiku, and G. Strobl, 1999, *New J. Phys.* **1**, 17.
- Heck, B., S. Siegenfuehr, G. Strobl, and R. Thomann, 2007, *Polymer* **48**, 1352.
- Hippler, T., S. Jiang, and G. Strobl, 2005, *Macromolecules* **38**, 9396.
- Hoffman, J., G. Davis, and J. Lauritzen, 1976, in *Treatise on Solid State Chemistry*, edited by N. B. Hannay (Plenum, New York), Vol. 3, p. 497.
- Hugel, T., G. Strobl, and R. Thomann, 1999, *Acta Polym.* **50**, 214.

- Imai, M., K. Kaji, T. Kanaya, and Y. Sakai, 1995, *Phys. Rev. B* **52**, 12696.
- Kanig, G., 1975, *Prog. Colloid Polym. Sci.* **57**, 176.
- Keller, A., M. Hikosaka, S. Rastogi, A. Toda, P. Barham, and G. Goldbeck-Wood, 1994, *J. Mater. Sci.* **29**, 2579.
- Li, C., L. Chan, K. Yeung, K. L. Y. Li, and J. X. Ng, 2001, *Macromolecules* **34**, 316.
- Magonov, S., and Y. Godovsky, 1999, *Am. Lab. (Shelton, Conn.)* **31**, 55.
- Michler, G., 1992, *Kunststoff-Mikromechanik* (Carl Hanser, Munich), p. 187.
- Minakov, A., D. Mordvintsev, and C. Schick, 2004, *Polymer* **45**, 3755.
- Olmsted, P., W. Poon, T. McLeish, T. Terrill, and A. Ryan, 1998, *Phys. Rev. Lett.* **81**, 373.
- Ostwald, W., 1897, *Z. Phys. Chem.* **22**, 286.
- Rastogi, S., M. Hikosaka, H. Kawabata, and A. Keller, 1991, *Macromolecules* **24**, 6384.
- Reiter, G., and G. Strobl, 2007, *Progress in Understanding of Polymer Crystallization*, Lecture Notes in Physics Vol. 714 (Springer, New York).
- Ruland, W., 1977, *Colloid Polym. Sci.* **255**, 417.
- Schmidtke, J., G. Strobl, and T. Thurn-Albrecht, 1997, *Macromolecules* **30**, 5804.
- Sirota, E., and A. Herhold, 1999, *Science* **283**, 529.
- Strobl, G., 2000, *Eur. Phys. J. E* **3**, 165.
- Strobl, G., 2006, *Prog. Polym. Sci.* **31**, 398.
- Strobl, G., 2007, *The Physics of Polymers*, 3rd ed. (Springer, New York), p. 165.
- Vaughan, A., and D. Bassett, 1989, *Comprehensive Polymer Science* (Pergamon, New York), Vol. 2, p. 415.
- Wunderlich, B., 1980, *Macromolecular Physics* (Academic, New York), Vol. 3, p. 58.